Journal of Polymers and the Environment
https://doi.org/10.1007/s10924-024-03460-w

ORIGINAL PAPER

In-situ Preparation of Highly Efficient Antibacterial Modified Pectin Using Zeolitic Imidazolate Framework

Hanieh Hamedi[1] · Jahanghir Azizi[1] · Siamak Javanbakht[1] · Reza Mohammadi[1]

Accepted: 20 November 2024

Abstract
With rising concerns about antibiotic resistance globally, exploring innovative antibacterial strategies is vital for public health. This work aimed innovatively to improve the biological efficacy of pectin (Pec) hydrogel beads by synergistically utilizing an antibacterial zeolitic imidazolate metal-organic framework (ZIF-8) and tetracycline (TC). ZIF-8 was incorporated at various concentrations within the hydrogel matrix to end this using an in-situ synthesis technique. TC was also pre-loaded into Pec hydrogel beads to further improve their antibacterial features. The application of diverse analysis techniques validated the successful fabrication of nanocomposites. In-vitro Zn^{2+} and TC release were considered by simulating the human digestive system, indicating a sustained and controlled release rate during 8 h (pH 1.2:6.8:7.4 = 20%:20%:60%). Antibacterial tests displayed inhibition zones of 14 ± 0.5 mm and 12 ± 0.5 mm against *Escherichia coli* and *Staphylococcus aureus* bacteria. Additionally, the MTT assay displayed potent cytotoxicity (> 70% cell viability after 48 h) for the human colon adenocarcinoma HT29 cell line. These results suggest that the developed nanocomposites have promising potential as an antibacterial bio-platform that is effective against resistant pathogens commonly found in the gastrointestinal tract.

Keywords Antibacterial · Drug Delivery · Hydrogel · Metal-organic Frameworks · Pectin

Introduction

In recent years, the global health landscape has been significantly impacted by the challenge of antibacterial resistance [1]. Conversely, the issue of antibiotic resistance has emerged as a significant concern primarily due to the widespread and often inappropriate utilization of traditional antibiotics, resulting in their diminishing effectiveness against microorganisms. This development has now escalated to become the second leading cause of mortality on a global scale. Hence, exploring innovative approaches is essential to enhance the management of bacterial infections, reduce adverse effects, and enhance the effectiveness of antibacterial agents [2]. This problem necessitates the progress of antibacterial drug delivery systems that can improve the specificity and bioactivity of antibacterial agents while reducing the probability of side effects [3]. Antibacterial agent delivery systems have attracted significant interest in restraining bacterial proliferation and enhancing drug effectiveness [4, 5].

In the last decade, because of their improved biocompatibility, biodegradability, and stability, biopolymers have become increasingly important for use in biomedical domains like drug delivery, tissue engineering, and gene delivery [6–8]. Natural polymers or composites based on polymers that are taken from fungi, bacteria, plants, and animals contain biopolymers [9]. Pectin, a naturally occurring polysaccharide found in the cell walls of higher plants, has been explored for its potential in the delivery of antibacterial drugs. Its unique properties, i.e., biocompatibility, biodegradability, non-toxicity, and ability to create gels, make it an attractive candidate for developing novel drug delivery systems [10]. Pectin has been employed in various pharmaceutical applications, including the delivery of bioactive substances for therapeutic purposes. Its ability to form gels and its swelling properties under physiological conditions make it suitable for developing controlled-release systems [10, 11]. Pectin-based hydrogels have been designed to deliver drugs to particular sites within the body, such as

✉ Reza Mohammadi
r.mohammadi@tabrizu.ac.ir

[1] Polymer Research Laboratory, Department of Organic and Biochemistry, Faculty of Chemistry, University of Tabriz, Tabriz, Iran

Published online: 28 November 2024

the colon, where they can target and eliminate pathogenic bacteria [12]. These hydrogels can be designed to release drugs in response to specific stimuli, such as changes in pH or temperature [13]. Research indicates that adding other elements to biopolymer matrices, like carbon nanotubes, metal-organic frameworks, nanoparticles, and double-layer hydroxides, can improve their performance [14, 15]. When biopolymers are combined with these materials, their properties, and potential uses are improved as much as possible [16, 17].

Crystalline metal-organic frameworks (MOFs) as low-density and porous materials are composed of organic bonds (organic ligands) and metal groups (clusters or metal ions) [18]. MOFs exhibit several properties, including tunable porosity, high surface area, chemical composition, and easy functionalization, that make them suitable for biomedical applications. Among the biomedical applications of MOFs, targeted drug delivery, stimulus-responsive release, biomedical imaging, and photodynamic therapy can be mentioned [19–21]. In addition, MOFs' biodegradability, biocompatibility, and drug-loading capacity make them promising candidates for use as antibacterial agents and drug carriers [22]. They are also appropriate for application in the field of antimicrobials owing to their lack of toxicity, robust pseudo-enzymatic activity, great surface area, and consistent discharge of bioactive ligands and metal ions.

Composites of MOFs and polymers are better prospects for biomedical applications than their pristine compounds because of the synergetic enhancement of biological properties [23–26]. On the other hand, the application of MOFs in biopolymer fillers has been deemed feasible [27]. These fillers influence the polymer's mechanical, electrical, thermal, strength, toughness, and porosity properties [28, 29]. Food packaging, water purification, medicine delivery, gas separation, and catalysis have all used the resultant nanocomposites [30].

Pectin acts as a natural polysaccharide that serves as a matrix for the nanocomposite, providing a biodegradable and biocompatible environment for incorporating other components like zeolitic imidazolate framework-8 (ZIF-8) and antibiotics (e.g., tetracycline). In the synthesis process, pectin facilitates crosslinking in a "green" medium (water and alcohol), which is crucial for forming stable hydrogel beads. Due to its unique structural and chemical properties, ZIF-8 plays a significant role in antibacterial applications. The zinc ions within ZIF-8 can be released into the surrounding environment, inhibiting bacterial growth. Additionally, imidazolate ligands, critical components in ZIF-8, exhibit notable antibacterial activity [31].

In-situ synthesis in the context of composites and hydrogels represents a significant advancement in materials science, particularly for developing multi-functional materials with enhanced properties. This approach involves the simultaneous formation of nanoparticles or other components within a polymer matrix or hydrogel, leading to unique structural and functional characteristics [32, 33]. This integrated approach enhances the uniformity and distribution of nanoparticles within the hydrogel, improving material properties. The main challenge in this field is the penetration of the cargoes within the MOF pores because they are attached to the exterior surface of MOFs, which affects the MOF porosity, loading efficiency, and release profile [34–36].

As far as we are aware, the in-situ synthesis approach has rarely been employed to create polysaccharide/MOF nanocomposite materials. In this study, we selected ZIF-8, a bio-MOF composed of biologically active metal ions and ligands, due to its potential for developing innovative antibacterial strategies [37]. It is crucial to explore more environmentally friendly methods for synthesizing ZIF-8. To establish a unique combinatorial antibacterial platform, we synthesized ZIF-8 in situ and incorporated it into tetracycline (TC)-loaded Pec hydrogel beads crosslinked by Ca^{2+} using green solvents (i.e., water and alcohol). This approach allows us to investigate the synergistic effects of pectin, zinc ions (Zn^{2+}), and TC biomolecules on enhancing the antibacterial properties of the nanocomposite hydrogel beads. Ultimately, this research aims to create an effective bioplatform for antibacterial applications, particularly in colon cells, addressing the pressing need for targeted therapeutic strategies against gastrointestinal infections. The colon is a significant site for various infections and diseases, including inflammatory bowel disease and colorectal cancer. Developing antibacterial agents specifically for colon cells can enhance targeted delivery, ensuring that therapeutic agents effectively reach the intended site of action.

Experimental

Materials

Pectin (50–75% esterification, ≥ 90.0 %, solubility water: 0.02 g/10 mL) was provided from Sigma–Aldrich Co. Zinc nitrate hexahydrate ($Zn(NO_3)_2.6H_2O$, ≥ 98.0 %), 2-Methylimidazole (2-MeIM, ≥ 99.0 %), Calcium chloride ($CaCl_2$, ≥ 99.0 %), and all other chemicals were attained from Sigma Aldrich Co. (Germany). Tetracycline (TC, ≥ 99.0 %) was attained from Exir Pharmaceutical Co. (Iran). All biological reagents were obtained from Invitrogen Co. (USA).

Characterization

Using a Bruker spectrophotometer, the samples' Fourier transform infrared (FT-IR) spectra were documented at

Table 1 Desired amounts of starting materials for preparing hydrogel beads

Beads	Starting materials								
	H_2O (mL)	TC (mg)	2-MeIM (mg)	Pec (mg)	Glycerol (μL)	H_2O (mL)	C_2H_5OH (mL)	$CaCL_22H_2O$ (mg)	$Zn(NO_3)_2$ $6H_2O$ (mg)
Pec	3	-	-	200	8	2	2	0.4	-
Pec/ZIF-8 (1)	3	20	227	200	8	2	2	0.4	11
Pec/ZIF-8 (1)	3	20	227	200	8	2	2	0.4	110
TC-Pec	3	20	-	200	8	2	2	0.4	-
TC-Pec/ ZIF-8 (1)	3	20	227	200	8	2	2	0.4	11
TC-Pec/ ZIF-8 (2)	3	20	227	200	8	2	2	0.4	110

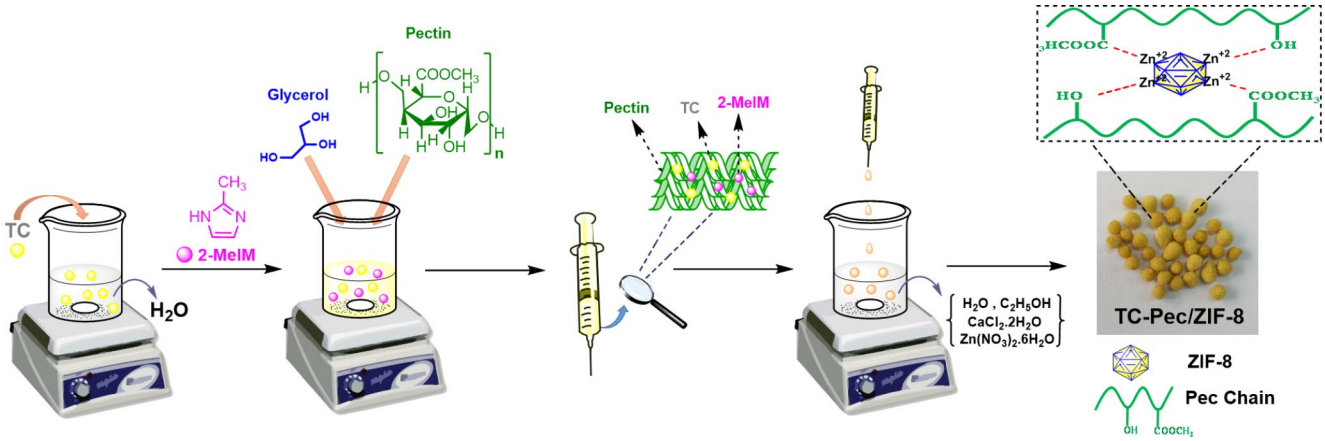

Fig. 1 Schematic procedure for preparation of TC-Pec/ZIF-8 nanocomposite hydrogel bead

room temperature using KBr tablet in the 400–4000 cm^{-1} range. An instrument used for ultraviolet-visible (UV-Vis) measurements was a Shimadzu UV-2100 spectrophotometer for determining TC concentration. The NovaAA-400 atomic absorption spectrophotometer was used to measure atomic absorption to determine Zn^{2+} concentration. A LEO 1455VP scanning microscope and scanning electron microscopy (SEM) were used to record the morphologies of the synthesized samples after coating them with a gold layer. The produced hydrogel beads were subjected to elemental analysis *via* energy-dispersive X-ray spectroscopy (EDX) at room temperature. Using a Bruker D8 Advance diffractometer, the compounds' X-ray diffraction (XRD) pattern was captured at room temperature in the 2θ range 5–65°. The pH of the aqueous solutions was calibrated using a HI2211 pH/ORP meter (HANNA model, Iran).

Synthesis of Nanocomposite Hydrogel Beads

The different concentrations of Pec, Zn, and 2-MeIM were considered to prepare the hydrogel beads (Table 1). TC solution was first prepared for the initial drug loading. Next, 2-MeIM, Pec, and glycerol were added to the above solution and stirred at 300 rpm. After creating a second mixture with 50% ethanol and water, a specific amount of $Zn(NO_3)_2.6H_2O$ and $CaCl_2.2H_2O$ as a cross-linker was added. The final step involved adding the first mixture to the second mixture drop by drop to create hydrogel beads, as seen in Fig. 1. ZIF-8 crystals are in-situ grown inside the Pec network by diffusion of Zn^{2+} into the Pec matrix containing 2-MeIM to construct the TC-Pec/ZIF-8 nanocomposite hydrogel bead [37]. The beads were immersed in the second mixture for 24 h. UV analysis was conducted to determine the quantity of drug released into the crosslinked medium. This amount was subtracted from the initial pre-loaded drug quantity to ascertain the final amount of drug remaining in the beads. Subsequently, the beads underwent three washing cycles and were then dried. The TC loading efficiency was determined using Eq. 1.

$$\text{TC loading efficiency } (\%) = \frac{Mass\ of\ drug\ in\ beads}{Mass\ of\ drug\ fed\ initially} \times 100 \quad (1)$$

In-vitro Swelling and erosion Studies

The swelling and erosion features of the hydrogel beads (Pec, Pec/ZIF-8 (1), and Pec/ZIF-8 (2)) were tested in solutions of different pH levels (1.2, 6.8, and 7.4). The dried samples at 45 °C were weighed (8 mg) in 10 mL buffered solution. After blotting the swollen beads with filter paper

Table 2 The result of the TC release profile fitting with different kinetics models

Kinetic models	Equations	R^2		
		TC-Pec	TC-Pec/ZIF-8(1)	TC-Pec/ZIF-8(2)
Zero-order	F= k_0t	0.8022	0.6200	0.5652
First-order	$\ln(1-F) = k_f t$	0.8310	0.6322	0.5692
Higuchi	$F = k_H\sqrt{t}$	0.8586	0.7708	0.7171
Weibull	$\ln[-\ln(1-F)] = -\beta \ln t_d + \beta \ln t$	0.9433	0.8502	0.8123

k_0, $k_f$and k_H are the kinetic constants of respective models, Ln is the natural logarithm, and F is the fraction of drug released up to time t

Table 3 The result of fitting the Zn^{+2} release profile with different kinetics models

Kinetic models	Equations	R^2	
		Pec/ZIF-8(1)	Pec/ZIF-8(2)
Zero-order	F= k_0t	0.5240	0.3926
First-order	$\ln(1-F) = k_f t$	0.5247	0.3934
Higuchi	$F = k_H\sqrt{t}$	0.6908	0.5880
Weibull	$\ln[-\ln(1-F)] = -\beta \ln t_d + \beta \ln t$	0.8400	0.8195

k_0, k_f and k_H are the kinetic constants of respective models, Ln is the natural logarithm, and F is the fraction of drug released up to time t.

to remove surface water, the beads were removed at specific intervals and weighed again. An increase in weight was considered swelling, while a decrease in weight (after drying at ambient temperature) was considered erosion [22]. The swelling and erosion percentages were calculated with Eqs. 2 and 3:

$$Swelling\ (\%) = \left(\frac{W_s - W_i}{W_i}\right) \times\ 100 \tag{2}$$

$$Erosion\ (\%) = \left(\frac{W_i - W_d}{W_i}\right) \times\ 100 \tag{3}$$

where W_i, W_s, and W_d are the weights of the initial, swollen, and dry samples, respectively.

pHpzc Determination

The pH value at which the particles' net surface charge is zero is typically used to calculate the pH_{pzc} [38]. Samples with varying alkaline and acidic pHs were mechanically mixed to determine pH_{pzc}. Then, pH_{pzc} is obtained by the difference between the final and initial pH from Eq. 4. At pH_{pzc}, the difference between the initial and final pH (ΔpH) is zero.

$$\Delta\, pH = pH_{final} - pH_{initial} \tag{4}$$

In-vitro drug Release

In-vitro drug release tests were carried out using previously reported methods with some modifications [38]. 50 mg of the prepared dried samples were successively immersed, and they were capped in a dialysis bag in a 10 mL buffer solution in an environment with pH 1.2, 6.8, and 7.4, which respectively simulate the pH of gastric fluid, the first region of the intestinal fluid, and the second region of the intestinal fluid [39]. Initially, it was immersed at pH 1.2 for 2 h, then transferred to pH 6.8 for 2 h, and finally to pH 7.4 for 4 h. A satisfactory volume of supernatant (2 mL) was extracted at designated time points, while an equal volume of new buffer was introduced to maintain a consistent buffer volume. Drug release was quantified using a UV-Vis spectrophotometer at 276 nm, and the calibration of Zn^{2+} was assessed through atomic absorption analysis. Finally, the percentage of TC and Zn^{2+} released was determined using the following Eq. 5 and Eq. 6, respectively:

$$TC\ release\ (\%) = \frac{the\ amount\ of\ reased\ TC}{the\ amount\ of\ loaded\ TC} \times\ 100 \tag{5}$$

$$TC\ releasese\ (mg/g) = \frac{the\ amount\ of\ reased\ Zn^{2+}}{the\ amount\ of\ carrier} \tag{6}$$

In addition, the release profile is fitted with different kinetic models [40], and the release kinetics were assessed as summarized in Tables 2 and 3. All fitting is considered by linear regression.

Antibacterial Study

The antibacterial efficacy of the hydrogels was evaluated through the disc diffusion technique against two bacterial strains, i.e., *Staphylococcus aureus* (*S. aureus*) and *Escherichia coli* (*E. coli*) [41]. In this regard, 50 µL of bacterial spore suspensions (1×10^4 cells/mL) were added to the agar plates. Next, the hydrogel beads were layered atop the agar. The plates were kept in a 37 °C incubator all night. After that, a ruler measured the diameter of the inhibitory zones' appearance.

In-vitro Cytotoxicity

The cytotoxicity of Pec, ZIF-8, Pec/ZIF-8 (1), Pec/ZIF-8 (2), TC-Pec, TC-Pec/ZIF-8 (1), and TC-Pec/ZIF-8 (2) towards the human colon adenocarcinoma HT29 cell line was investigated using the MTT assay, following the method that has been reported [42]. In short, the beads were exposed to 70% ethanol for 5 min to sterilize them, and then they were subjected to UV light for 20 min. The samples were washed twice with PBS (pH 7.4) and soaked in a new culture medium. After twenty-four hours, the human colon adenocarcinoma HT29 cell line was grown in triplicate at a density of 10^4 cells per well into 96-well plates (containing samples). As the control group, cells without samples that received only fresh media were employed. After replacing the media with 150 µL of fresh culture medium containing MTT solution (5 mg mL^{-1}), the formazan crystals were dissolved by incubating the mixture for 4 hours at 37 °C. After removing the medium, 200µL of DMSO was added to dissolve the purple-blue MTT formazan precipitate. The absorbance of the solubilized formazan was measured using a multi-well plate reader (Quant Bio-Tek Instruments, Winooski, VT, USA) after 30 min. Percent cell viability was determined using Eq. 7:

$$Cell\ Viability\ (\%) = \frac{Reacted\ cells}{optical\ density\ of\ the\ control} \times 100 \quad (7)$$

Statistical Analysis

For the results, the data are displayed as mean ± standard deviation. One-way analysis of variance (ANOVA) was used to conduct statistical analysis using Microsoft Excel software, with a $P < 0.05$ threshold for statistical significance. Three experiments were considered for each test.

Results and Discussion

Preparation of Nanocomposite Hydrogel Beads

The present study employed the in-situ synthesis method, a straightforward, inexpensive, and biocompatible technique to grow ZIF-8 in Pec hydrogel beads. In this method, a coordinate bond can be created between Pec and the in-situ formed ZIF-8, forming the Pec/ZIF-8 nanocomposite hydrogel beads. On the other hand, this was made possible by hydroxyl and carboxyl groups in the Pec structure, which can easily coordinate with Zn^{2+} sites in the ZIF-8 framework. To end this, a drop-by-drop addition of the Pec and 2-MeIM mixture is made to the $Zn(NO_3)_2.6H_2O$ and $CaCL_2$ solution mixture. The resulting beads are allowed to rest at room temperature in the secondary mixture overnight (Fig. 1). As a result, the prepared Pec/ZIF-8 bio-platform as a cytocompatibility, affordable, and environmentally benign carrier was considered for TC and Zn^{+2} delivery to afford a controlled release profile.

FT-IR Analysis

The FT-IR analysis on the ZIF-8 in-situ synthesis in the Pec polymer matrix (Fig. 2A), as well as the pre-load of the TC drug (Fig. 2B), was evaluated to show the presence of functional groups and to examine interactions between the synthesized substances. In the FT-IR spectrum corresponding to the Pec/ZIF-8, the band appears in the (688 and 757) cm^{-1} regions, respectively, corresponding to the Zn-N and the Zn-O tensile vibrations present in the ZIF-8 structure, which confirms the creation of the ZIF-8 in the Pec polymer matrix. The bands in the 1151 cm^{-1} and 1330 cm^{-1} regions are related to the tensile vibrations of the C-N bonds in the 2-MeIM structure. The bending vibrations of the N-H bond appear at 1623 cm^{-1}, and the high-intensity band is reduced according to the vibrations of the carbonyl group (C = O) at 1735 cm^{-1} in the Pec/ZIF-8 spectrum compared to the pure Pec. This contribution can indicate the presence of interactions between the carbonyl group and ZIF-8. The band in 2920 cm^{-1} is related to aliphatic C-H tensile vibrations, and the wide band in 3100–3500 cm^{-1} is attributed to the O(N)-H vibrations of the Pec and 2-MeIM, as well as intermolecular hydrogen bonds. In the spectrum corresponding to pure Pec, C = O tensile vibrations appeared at 1735 cm^{-1}, C-H aliphatic tensile vibrations at 2923 cm^{-1}, and C-O tensile vibrations at 1050–1200 cm^{-1}.

The FT-IR spectrum for TC showed the absorption band for the N-H and O-H tensile vibrations at 3363 cm^{-1} and 3296 cm^{-1} and the C-H aromatic and aliphatic traction, respectively, at 3066 cm^{-1} and 2981 cm^{-1}. The vibration bands at 1675–1520 cm^{-1} were related to the C = C

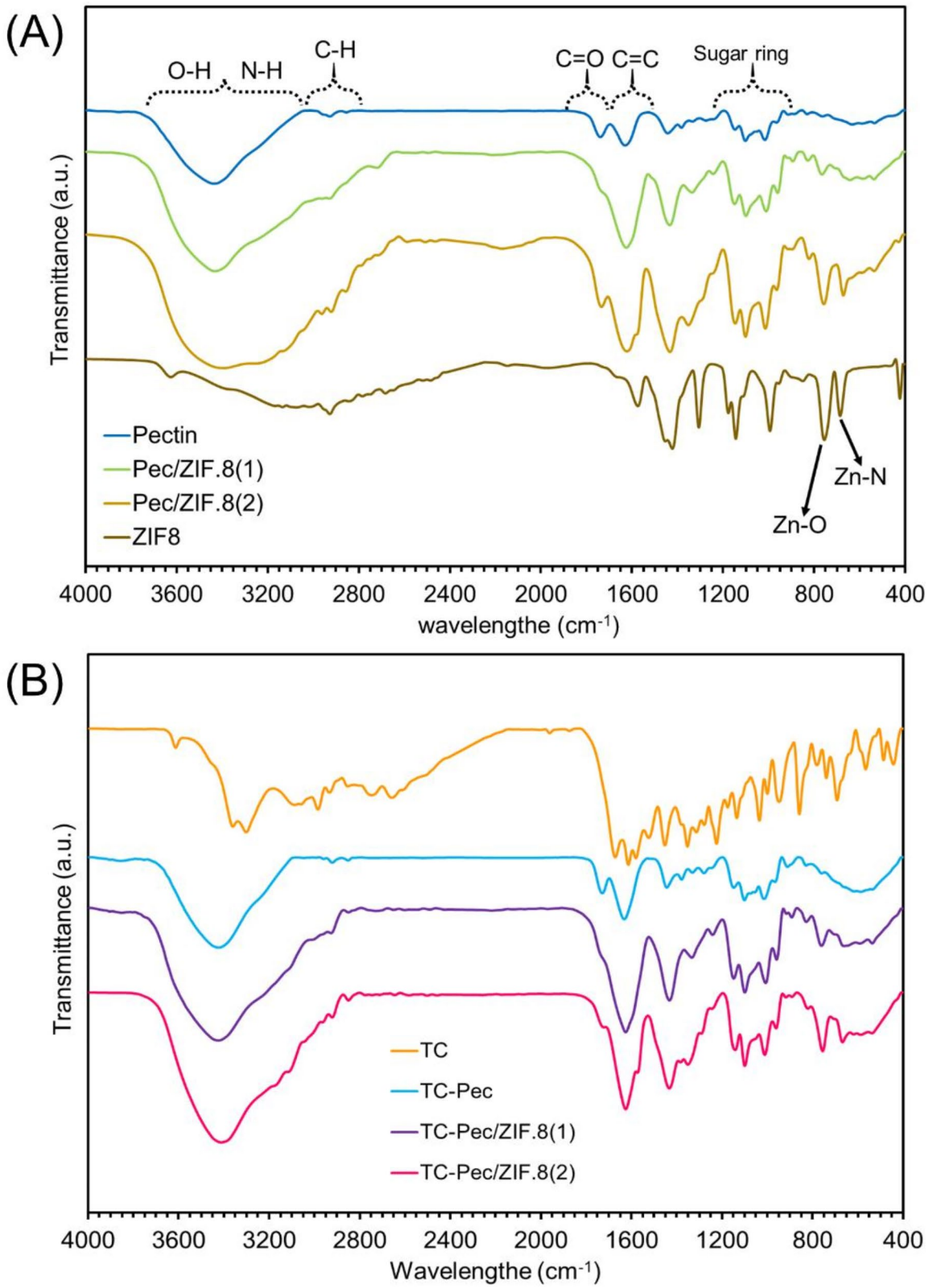

Fig. 2 FT-IR spectra for the (**A**) ZIF-8, Pec, Pec-ZIF-8(1), Pec/ZIF-8(2), and (**B**) TC, TC-Pec, TC-Pec/ZIF-8(1), TC-Pec/ZIF-8(2)

vibration, and the aromatic bending vibrations of C-H appeared at 1452 cm^{-1} and the aliphatic bending of C-H at 1352 cm^{-1}. Aromatic deformation picks inside and outside the screen at 1224–1000 cm^{-1} and 570 – 500 cm^{-1} appeared. The vibration band at 948 cm^{-1} was assigned to the C-N vibration. However, after loading the TC drug, the appearance and variation of the intensity of the bands in the spectrum related to TC-Pec/ZIF-8 compared to the Pec/ZIF-8 spectrum can show a possible chemical interaction between the hydroxyl groups of the Pec/ZIF-8 structure and the amino groups of TC [43–46].

XRD Analysis

XRD patterns for ZIF-8, Pec, Pec/ZIF-8(1), and Pec/ZIF-8(2) are shown in Fig. 3. The appearance of 2θ diffraction peaks at 7.50°, 10.44°, 12.82°, 14.78°, 16.52°, 18.10°, 22.2°, 24.60°, and 29.70° confirms the successful synthesis of ZIF-8 [47]. XRD pattern of synthesized Pec hydrogel shows a polysaccharide's characteristic amorphous nature at 2θ about 20°, corresponding to the Pec network microstructure [48]. Although ZIF-8 exhibits a crystalline structure (JCPDS 00–062-1030) [49, 50], it exerts minimal influence on the amorphous structure of Pec polysaccharide. This phenomenon is likely attributed to the limited aggregation and effective dispersion of ZIF-8 nanoparticles within the nanocomposite structure.

pHpzc Analysis

The pH of the adsorbent solution is usually employed to determine the surface charge of the particles and their surface charge in the solution. It is commonly recognized that when the pH of an adsorbent solution is less than pH_{pzc}, the net charge on the particle surface is positive, and when the pH is higher, it is negative [51]. The zero-point potentials in Pec, Pec/ZIF-8(1), Pec/ZIF-8(2), and ZIF-8 are calculated at 4.1, 8.1, 8.2, and 9.8, respectively, as shown in (Fig. 4). With increasing the amount of ZIF-8 in the composition of hydrogel nanocomposites, pH_{pzc} was slightly increased. These results can prove successful ZIF-8 integration into Pec hydrogel beads.

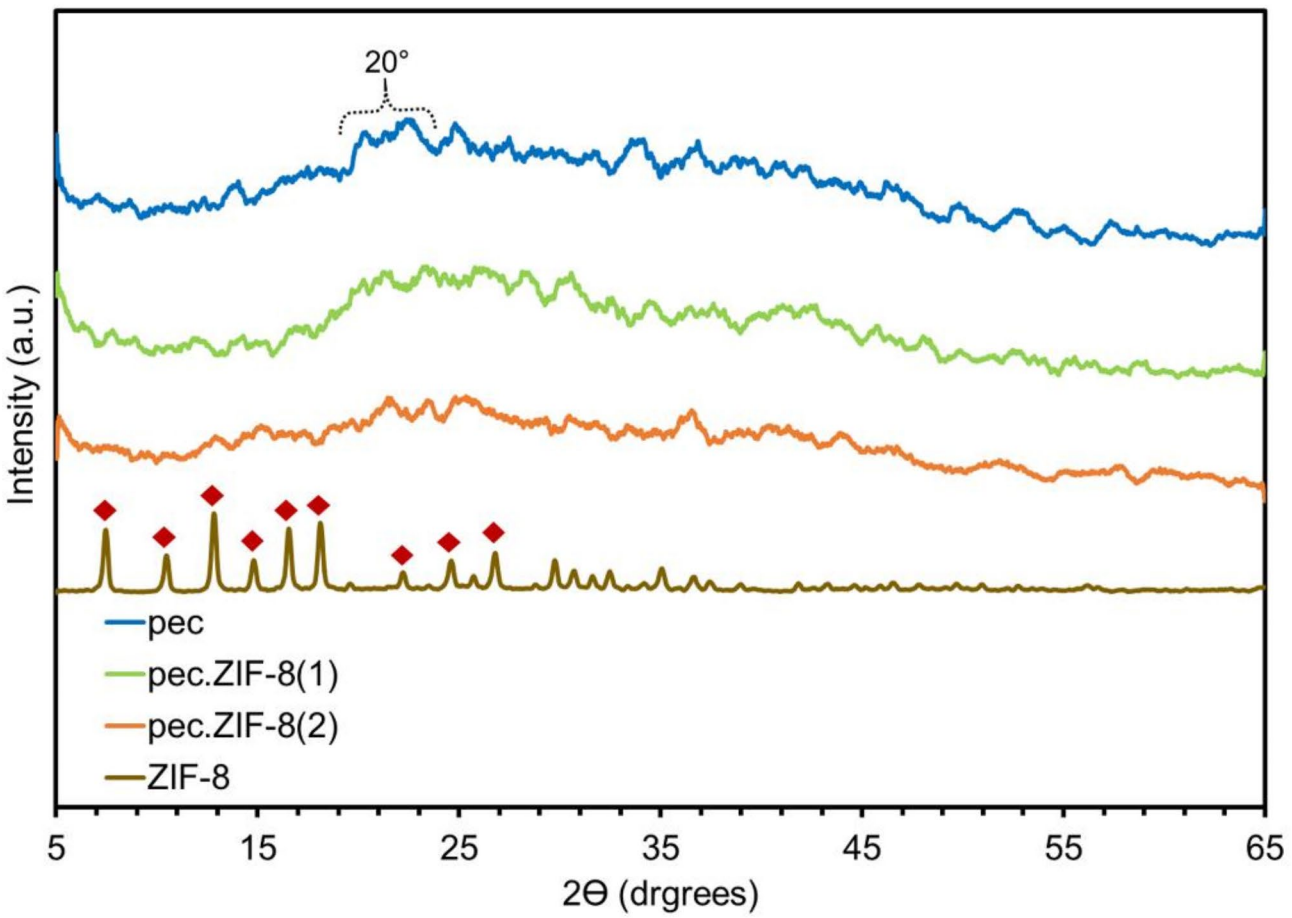

Fig. 3 The XRD patterns of ZIF-8, Pec, Pec/ZIF-8(1), and Pec/ZIF-8(2)

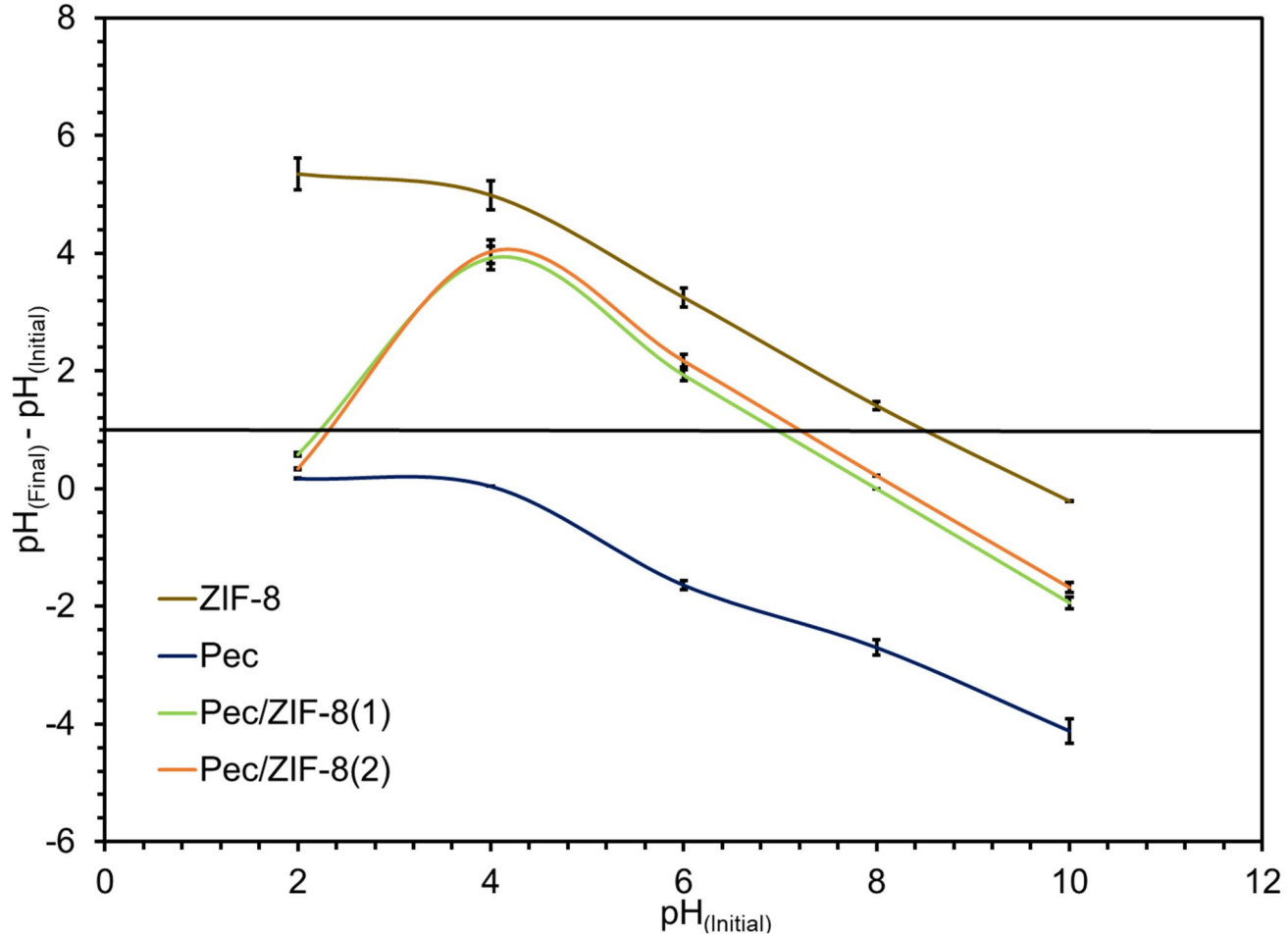

Fig. 4 pH_{pzc} of the Pec, Pec/ZIF-8(1), Pec/ZIF-8(2), and ZIF-8. The values are reported as mean ± SD of three experiments

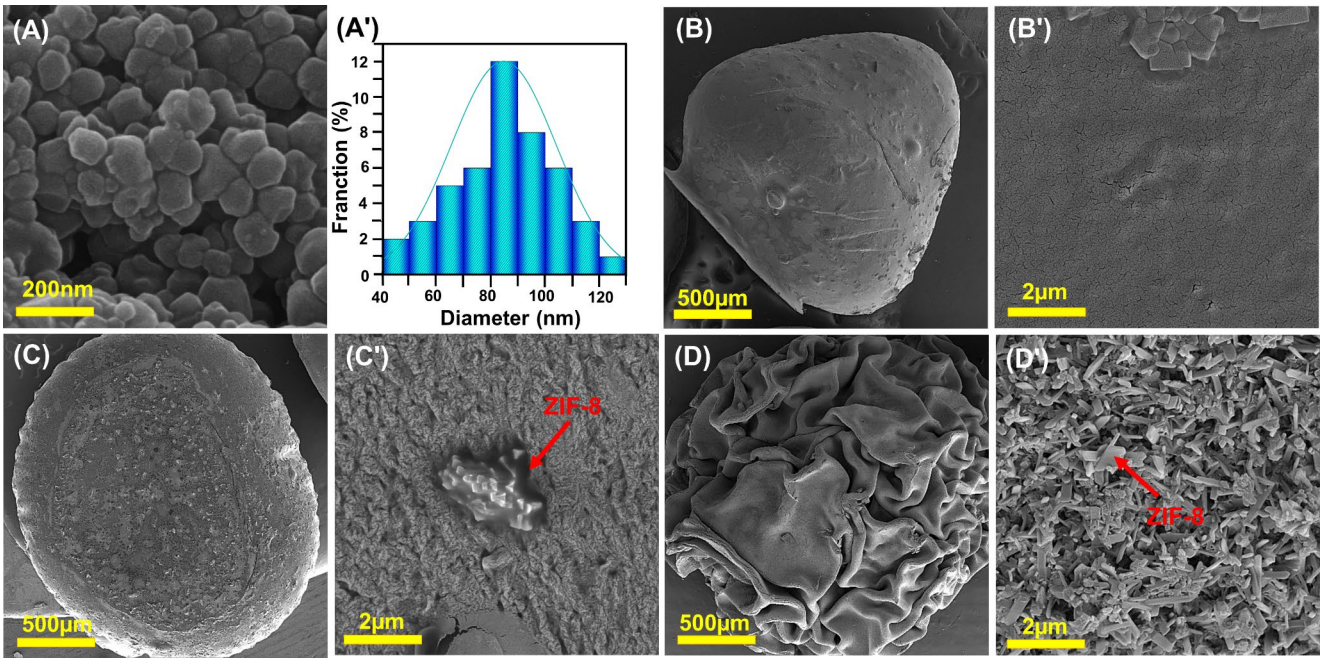

Fig. 5 SEM images of the (**A** and **A'**) ZIF-8 and Histogram of ZIF-8, (**B** and **B'**) Pec, (**C** and **C'**) Pec/ZIF-8(1), (**D** and **D'**) Pec/ZIF-8(2)

Morphological Analysis

The structure of the drug carrier plays a significant role in determining the drug release process. The morphology of ZIF-8 nanoparticles is illustrated in Fig. 5A, indicating a consistent and nearly spherical shape with a particle size of 90 nm determined using ImageJ software (as depicted in Fig. 5A'). Conversely, Blank Pec Hydrogel beads exhibit an almost spherical morphology of approximately 2 mm, featuring a folded and porous surface composition (Fig. 5B). The introduction of ZIF-8 nanoparticles to the hydrogel alters the surface morphology of the beads, as depicted in Fig. 5C-D. Furthermore, a comparison of hydrogel beads produced with varying concentrations of ZIF-8 reveals an increased dispersion of surface particles (Fig. 5C'-D'), likely attributed to the integration of ZIF-8 in the nanocomposite structure. The porosity of the synthesized beads was investigated using the method described in the supporting information. 4% ± 0.5, 8% ± 0.5, and 13% ± 0.5 were calculated for Pec, Pec/ZIF-8(1), and Pec/ZIF-8(2), respectively. Therefore, according to the SEM images, the porosity increases with the ZIF-8 concentration due to rising wrinkles and holes.

Elemental Mapping and EDX analyses confirm a uniform distribution of C, O, N, and Zn elements across the nanocomposite hydrogel bead structure, indicating a consistent in-situ synthesis of ZIF-8 nanoparticles (Fig. 6). In addition, DLS was utilized for determining the zeta potential of the synthesized materials. All of the tested samples show a positive charge, and this charge value is increased up to about 10 mV by incorporating ZIF-8 into the hydrogel matrix (Fig. 7).

Swelling and erosion Studies

The swelling of hydrogels can be seen as a confirmation of their crosslinking [52]. The swelling behavior of Pec and Pec/ZIF-8 hydrogel beads in the simulated stomach environment, first zone, and second zone of the intestine at pH 1.2, 6.8, and 7.4 have been investigated. At pH 1.2, protonation of carboxylate groups reduces the swelling capacity of the Pec-based hydrogel beads. In fact, due to the establishment of intramolecular hydrogen bonds, the hydrogel swells to a lesser extent [42]. In the following hours, when the environment's acidity decreases, and the hydrogel beads are placed at pH 6.8, the carboxylic acid groups of Pec lose their hydrogens, creating the Coulombic repulsion between the polymer chains. As a result, hydrogel absorbs more water, and hydrogen bonds between water molecules and acidic groups are created. In an environment with a pH of 7.4 (simulating the intestinal environment), the swelling rate will increase more because the acid groups are more ionized, and the amount of hydrogen bond formation increases. The swelling in an environment with a pH of 7.4 after 4 h reaches its maximum value. After 6 h, the hydrogel beads are completely destroyed in the intestinal environment. This phenomenon is due to the release of divalent calcium ions and their displacement with phosphate and potassium ions in the environment. As a result, the crosslinking bonds are destroyed, and the hydrogel is dissolved in the buffer. Also, the integration of ZIF-8 led to the formation of an additional three-dimensional structure in the Pec network, which was probably due to its possible interactions with Zn^{2+} sites of ZIF-8, and this factor led to a reduction in swelling. The swelling percentage, as shown in Fig. 8A, has partially decreased due to increasing the amount of ZIF-8. Instead, further increasing ZIF-8 into the polymeric network can disrupt the polymer structure's order and reduce swelling in Pec/ZIF-8(2) compared to Pec/ZIF-8(1). According to the results, integrating ZIF-8 into hydrogels increased their strength. As a result, their erosion decreased (Fig. 8B). According to the swelling rate, the degree of crosslinking can be concluded to be Pec < Pec/ZIF-8 (2) < Pec/ZIF-8 (1). This result is in accordance with the swelling results that revealed the crosslinking ability of ZIF-8. With the increase in ZIF-8 concentration, the degree of crosslinking increased; however, further incorporating the ZIF-8 nanoparticles diminished the crosslinking degree.

TC and Zn2+ Release Study

The TC loading efficiency was determined to be 83%, 92%, and 93% for Pec, Pec/ZIF-8(1) and Pec/ZIF-8(2), respectively. The TC release test was conducted in vitro by simulating the human digestive system to prove the potential of hydrogel beads prepared as carriers. The results show that the release of the drug depends on changes in time and pH (Fig. 9A). The rate of TC release in the buffered media with pH 1.2 (gastric environment simulator) is the lowest (less than 30%) compared to other environments. This contribution indicates that the hydrogel beads have good strength and can preserve the drug in the acidic media of the stomach and preserve the TC drug until it reaches its destination. The release rate of the drug increases over time and is higher at pH 6.8 than at pH 1.2. At pH 7.4, this rate increases due to swelling and the osmotic pressure of the environment. The release rate is at its highest rate in the first 4.5 h, and all the loaded drug is released. After about 4.5 h, the percentage of drug release remains constant, indicating the release process's end. The intestinal environment contains various enzymes, including pectinase [53]. Pectinase enzymes break down the Pec in the intestinal environment and degrade the hydrogel beads' structure, eventually releasing TC. In addition, the behavior of releasing Zn^{2+} was investigated by

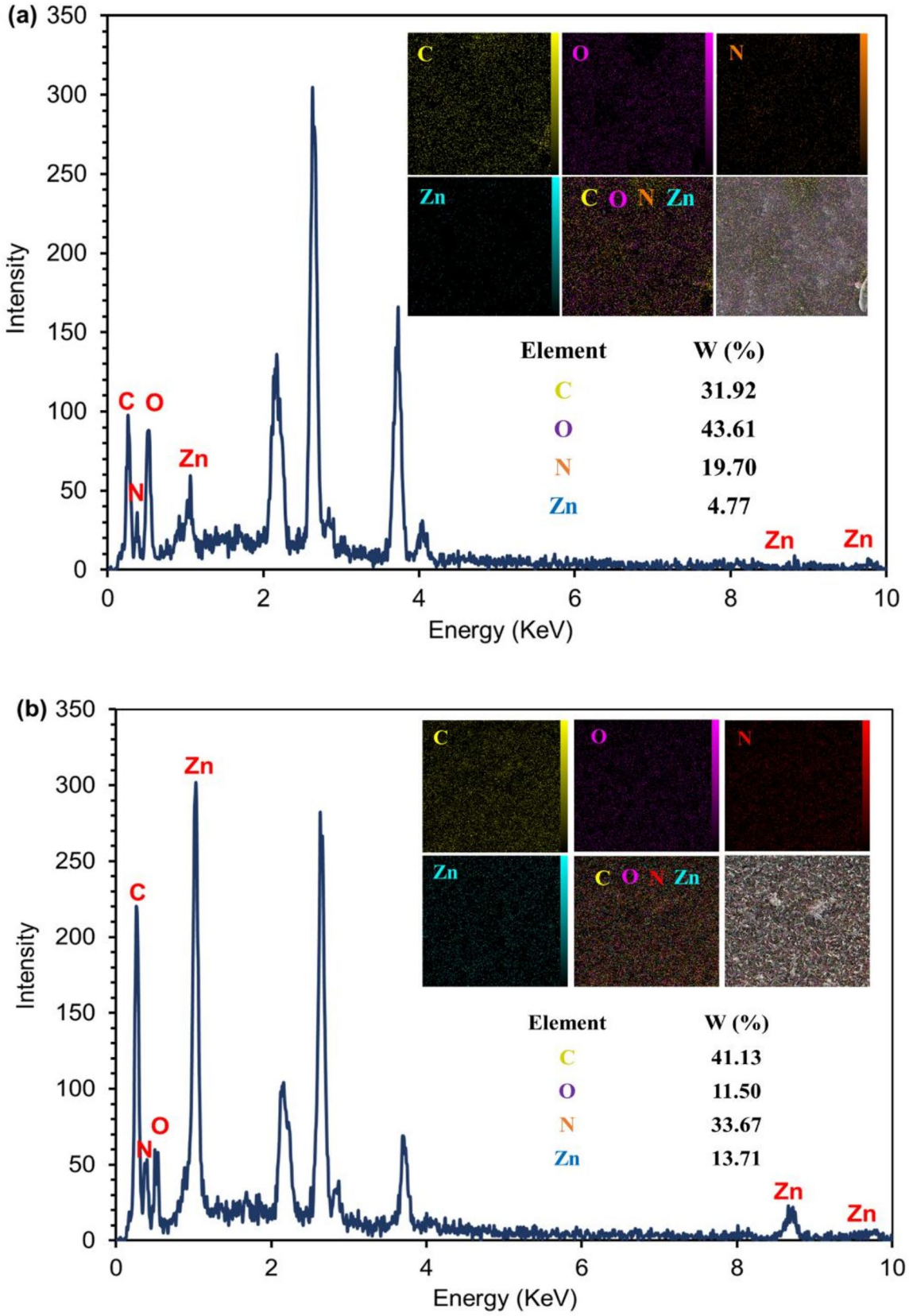

Fig. 6 Map images and EDX spectra of the (**a**) Pec/ZIF-8(1), and (**b**) Pec/ZIF-8(2

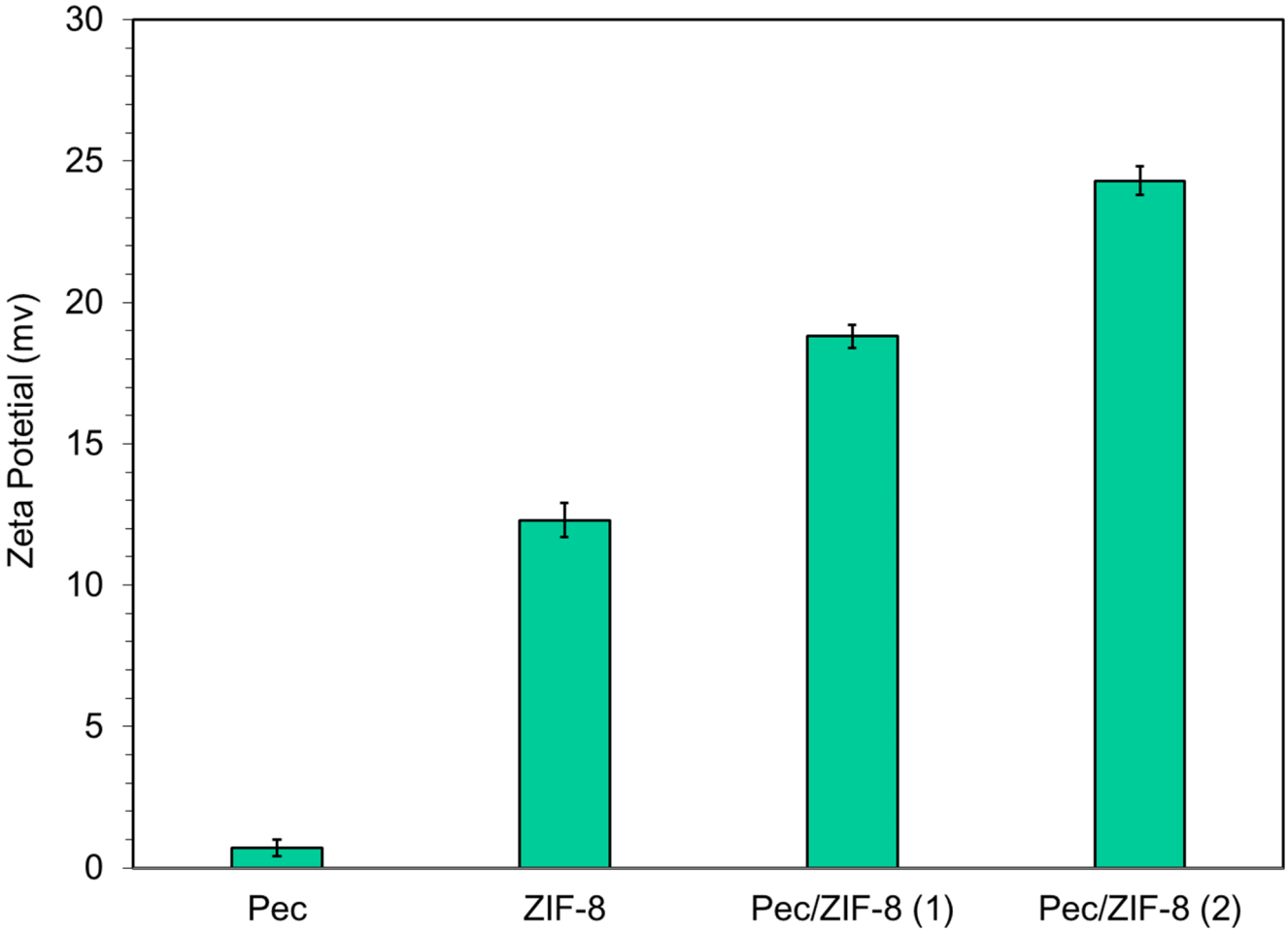

Fig. 7 Zeta potential of the Pec, ZIF-8, Pec/ZIF-8(1), and Pec/ZIF-8(2)

simulating the human digestive system at pHs of 1.2, 6.8, and 7.4. The release rate of the Zn^{2+} increases over time. In a pH 7.4 environment, this rate increases due to destroying the polymeric network of hydrogel beads (Fig. 9B). The Weibull model presented the most suitable model for releasing TC and Zn^{2+} (Tables 2 and 3). Weibull analysis can be described to explain the cumulative fraction graphs of the solved sample against time [54]. The Weibull model is known for its ease of use and has been effectively utilized to analyze the dissolution profiles of various drug types. Nonetheless, it is fundamentally an empirical model, lacking the ability to offer a mechanistic understanding of kinetic properties involved in drug dissolution processes. This limitation means that while the model can describe data trends, it does not elucidate the underlying mechanisms driving them [55].

Antibacterial Activity

The antibacterial efficacy of the prepared beads was assessed against *S. aureus* and *E. coli* bacteria through the agar disc diffusion technique. A comprehensive overview of the overall inhibition zone diameter is presented in Table 4, alongside relevant illustrations. The findings demonstrate a correlation between the observed sample diameters and the drug (TC and Zn^{2+}) release characteristics. The antibacterial mechanism of ZIF-8 involves the release of Zn^{2+} ions, which can bind to proteins in bacterial cell walls and membranes, leading to inactivation [56]. Additionally, the 2-MeIM in ZIF-8 has been shown to defeat bacterial growth [57]. The antibacterial effect of TC is primarily due to its ability to inhibit protein synthesis by binding to the 30 S ribosomal subunit, thereby inhibiting the formation of a peptide chain. Additionally, TC may alter the cytoplasmic membrane of bacteria, causing leakage of intracellular components, such as nucleotides, from the cell and causing death [58–60]. Table 4 also shows that the amounts of ZIF-8 increased the antibacterial activity of all beads before TC-loading against both *S. aureus* and *E. coli* bacteria. Furthermore, the TC-loaded beads demonstrated antibacterial activity towards both bacteria and were even slightly more potent against *E. coli* than *S. aureus*. The increased antibacterial effectiveness of TC-loaded beads against *E. coli* compared to *S. aureus*

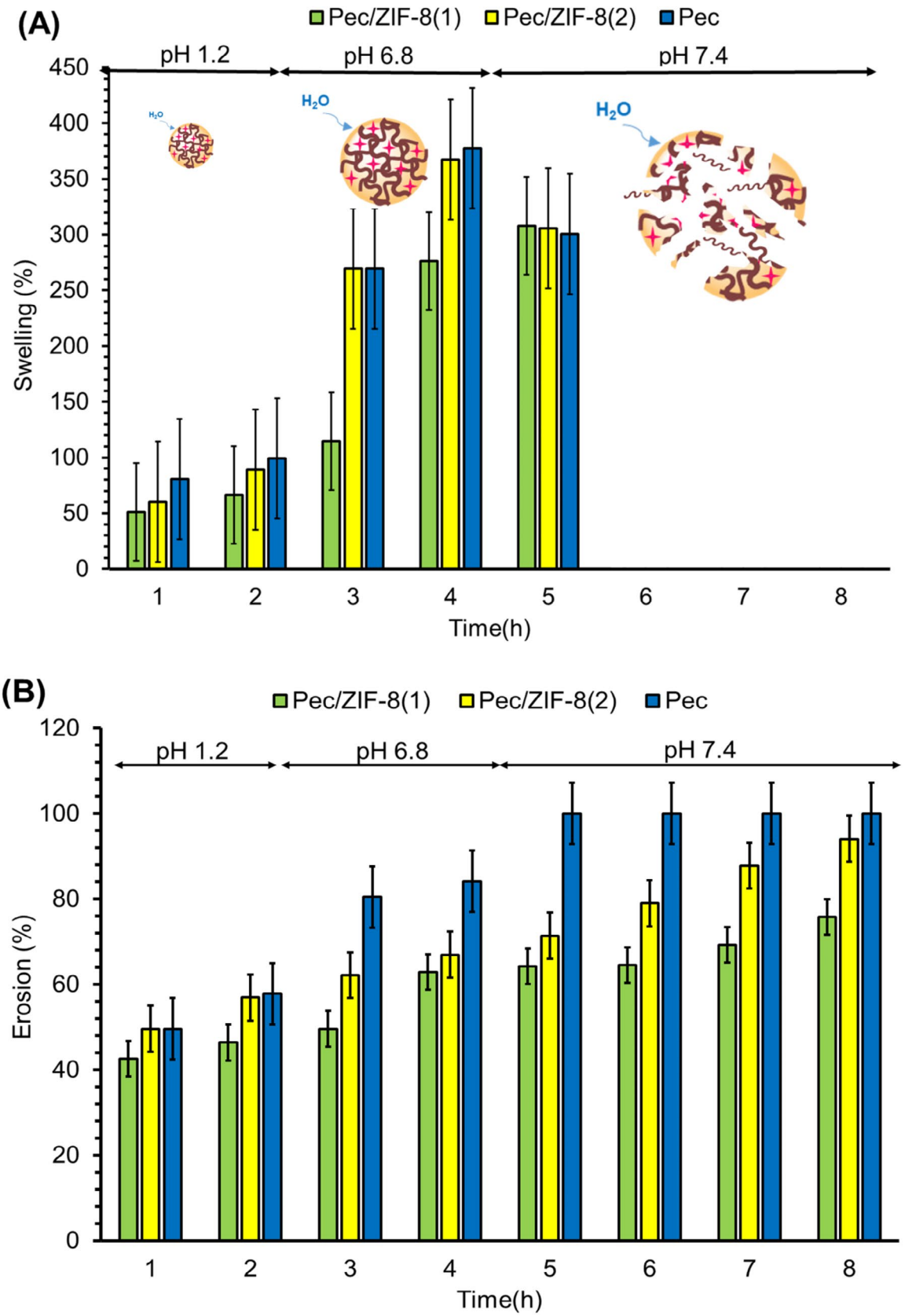

Fig. 8 (**A**) Swelling and (**B**) Erosion behavior of Pec-based nanocomposite hydrogel beads with different ZIF-8 concentrations at pH (1.2, 6.8, and 7.4) and 37 °C. The values are reported as mean ± SD of three experiments

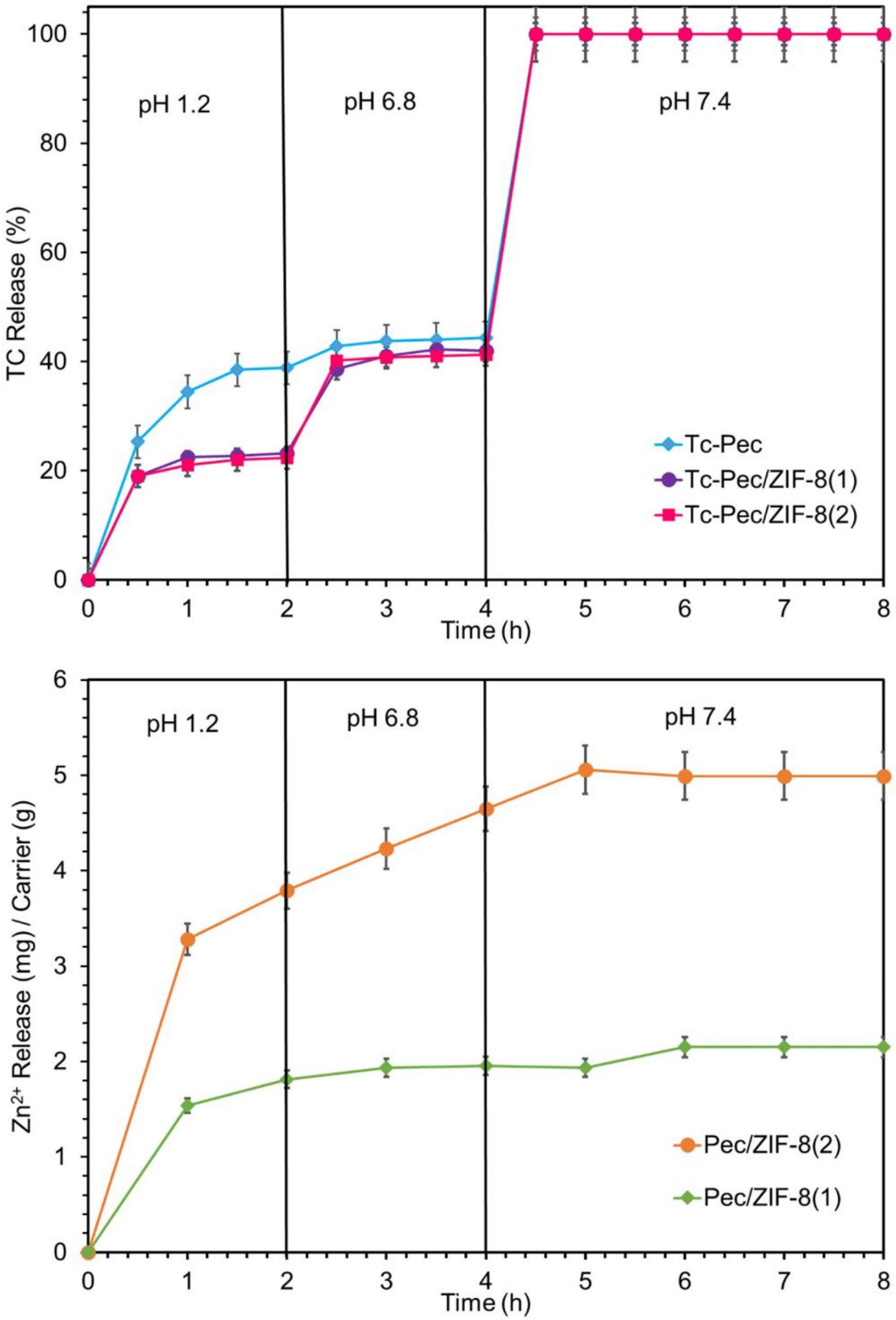

Fig. 9 TC and Zn^{2+} release behavior of Pec-based nanocomposite hydrogel beads with different ZIF-8 concentrations at pH (1.2, 6.8, and 7.4) and 37 °C. The values are reported as mean ± SD of three experiments

Sample	Inhibition zone diameter (mm)			
	S. aureus		*E. coli*	
ZIF-8	7 ± 0.5		12 ± 0.5	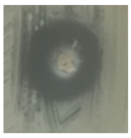
Pec	0 ± 0.5		0 ± 0.5	
Pec/ZIF-8 (1)	0 ± 0.5		0 ± 0.5	
Pec/ZIF-8 (2)	4 ± 0.5		7 ± 0.5	
TC-Pec	10 ± 0.5	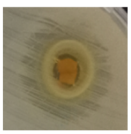	12 ± 0.5	
TC-Pec/ZIF-8 (1)	11 ± 0.5	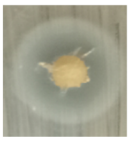	13 ± 0.5	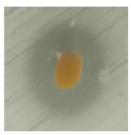
TC-Pec/ZIF-8 (2)	12 ± 0.5	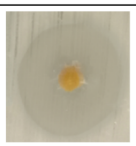	14 ± 0.5	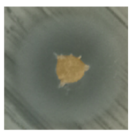

Table 4 Obtained data for the antibacterial activity of prepared beads against *S. Aureus* and *E. Coli* bacteria

is influenced by their structural differences and the mechanisms of the antibacterial agents. *E. coli*, a Gram-negative bacterium, has a thin peptidoglycan layer and an outer membrane that can hinder antibiotic susceptibility. In contrast, *S. aureus*, a Gram-positive bacterium, features a thick peptidoglycan layer that offers more protection [61–63]. TC works by inhibiting protein synthesis in both bacteria. However, *E. coli* has efflux pumps that reduce its susceptibility to TC, whereas *S. aureus* does not exhibit the same resistance level. The release of tetracycline and zinc ions (Zn^{2+}) from the beads may be more effective against *E. coli*, as zinc disrupts its cell membranes and metabolic functions more significantly than in *S. aureus*. Additionally, the synergistic effect of TC combined with metal ions like zinc enhances antibacterial activity against *E. coli*, similar to how silver ions show increased effectiveness against Gram-negative bacteria due to their ability to penetrate the outer membrane [64].

Cytotoxicity Study

The MTT test was used to measure the in-vitro cytotoxicity against human colon cell lines to determine the cytocompatibility of ZIF-8, Pec, Pec/ZIF-8(1), Pec/ZIF-8(2), TC-Pec, Pec/ZIF-8(1), and Pec/ZIF-8(2). Whereas incorporation of ZIF-8 reduced the cell viability in the polymeric Pec matrix, the cell viability of treated samples was still over 70% (Fig. 10). This result can be related to the cytocompatibility nature of Pec, which has been reported in the literature [49, 65]. Furthermore, TC loading does not significantly affect the cytotoxicity of hydrogel beads. Therefore, the TC-Pec/

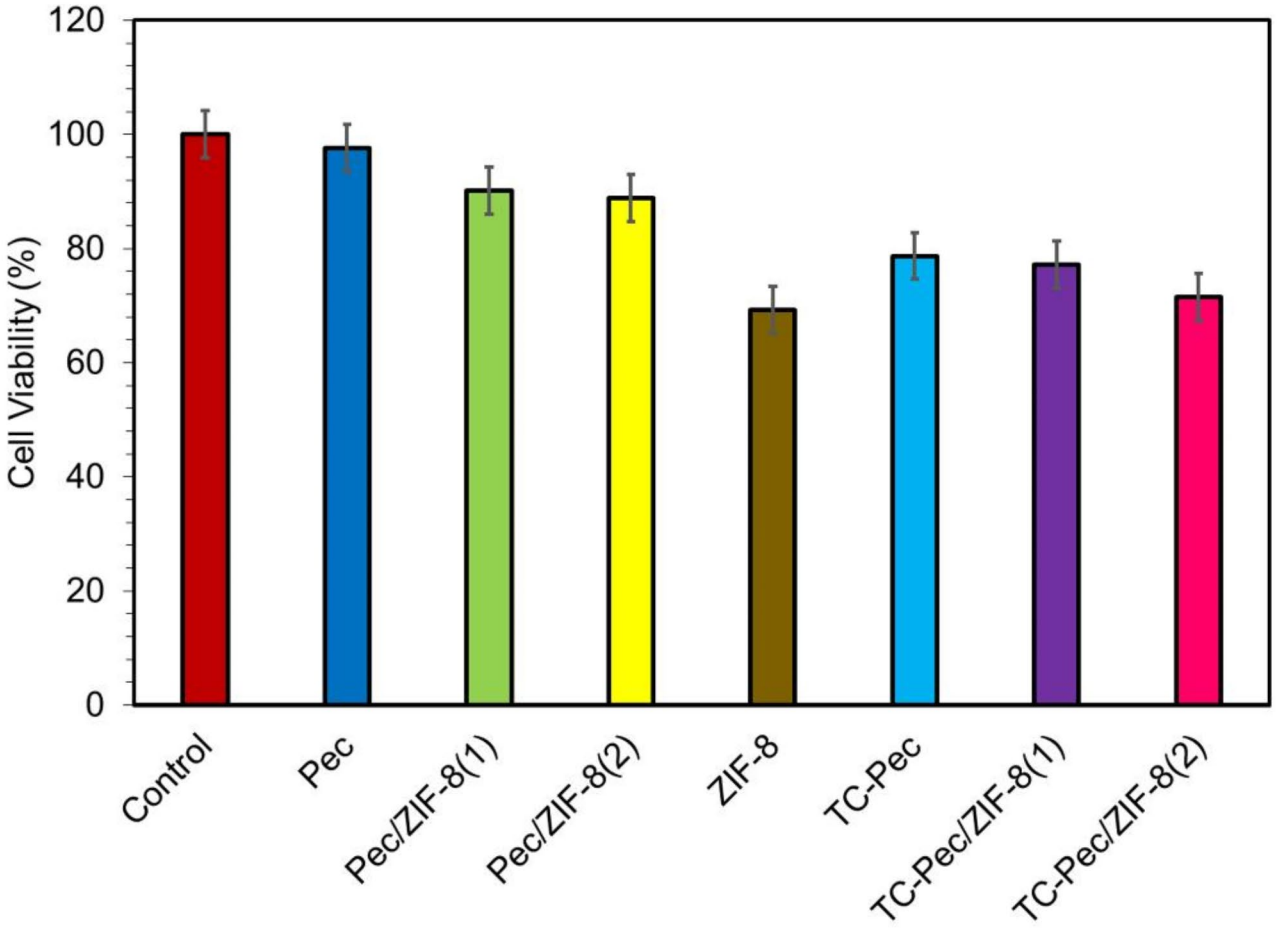

Fig. 10 Results of MTT assay on HT29 cells after 48 h incubation time with Pec, ZIF-8, Pec/ZIF-8 (1), Pec/ZIF-8 (2), TC-Pec, TC-Pec/ZIF-8 (1), and TC-Pec/ZIF-8 (2). Results are expressed as mean ± S.D. of three experiments

ZIF-8(2) platform can be a viable option for a safe antibacterial agent delivery system.

Conclusion

This study presents an innovative antibacterial oral delivery system utilizing Pec to develop antibacterial hydrogel beads with exceptional productivity through a straightforward method. The integration of ZIF-8 into the Pec network was successfully achieved via an in-situ synthesis approach. ZIF-8 possesses unique characteristics, including enhanced porosity, mechanical and chemical properties, thermal stability, and a high surface area, making it particularly effective for loading substantial amounts of TC and regulating its release profile. The development of these nanocomposite hydrogel beads benefits from the availability of precursors and the application of environmentally friendly methods, such as straightforward in-situ synthesis procedures. Incorporating ZIF-8 into the biopolymeric Pec network effectively controlled swelling, erosion, and release performance. However, it is important to note that excessive integration of ZIF-8 nanoparticles, which serve as cross-linkers, can reduce the nanocomposites' swelling ratio and erosion properties. For hydrogel beads containing ZIF-8, the release profiles of TC and Zn^{2+} exhibited a slight initial burst followed by a controlled release over 8 h (with a pH distribution of 1.2:6.8:7.4 at 20%:20%:60%). This behavior can be attributed to the diverse interactions between TC molecules and the nanocomposite. The Pec/ZIF-8 hydrogel beads demonstrated significant antibacterial activity against *E. coli* and *S. aureus*, with their antibacterial properties notably enhanced by incorporating TC, especially against *E. coli*. Among various formulations, TC-Pec/ZIF-8(2) exhibited higher antibacterial effects, showing inhibition zone diameters of 12 ± 0.5 mm for *S. aureus* and 14 ± 0.5 mm for *E. coli*. Additionally, these beads displayed cytocompatibility with approximately 70% cell viability in the human colon adenocarcinoma HT-29 cell line. Overall, the findings suggest that these hydrogel beads have significant potential as a

safe and straightforward system developed through an eco-friendly approach, serving as an effective antibacterial agent for treating intestinal infections.

Supplementary Information The online version contains supplementary material available at https://doi.org/10.1007/s10924-024-03460-w.

Acknowledgements This research is supported by the research grant of the University of Tabriz (number SAD/2389-14020820).

Author Contributions Conceptualization, H.H. and S.J.; methodology, H.H, and S.J.; validation, S.J. and R.M.; formal analysis, H.H. and J.A.; investigation, H.H. and J.A.; resources, R.M.; data curation, H.H.; writing—original draft preparation, H.H.; writing—review and editing, S.J. and R.M.; visualization, H.H.; supervision, R.M.; project ad-ministration, S.J.; All authors have read and agreed to the published version of the manuscript.

Data Availability The data that support the findings of this study are available from the corresponding author, upon reasonable request.

Declarations

Competing Interests The authors declare no competing interests.

References

1. Zhu X, Radovic-Moreno AF, Wu J, Langer R, Shi J (2014) Nanomedicine in the management of microbial infection–overview and perspectives. Nano Today 9(4):478–498
2. Osman N, Devnarain N, Omolo CA, Fasiku V, Jaglal Y, Govender T (2022) Surface modification of nano-drug delivery systems for enhancing antibiotic delivery and activity. Wiley Interdisciplinary Reviews: Nanomed Nanobiotechnol 14(1):e1758
3. Gao W, Chen Y, Zhang Y, Zhang Q, Zhang L (2018) Nanoparticle-based local antimicrobial drug delivery. Adv Drug Deliv Rev 127:46–57
4. Naahidi S, Jafari M, Edalat F, Raymond K, Khademhosseini A, Chen P (2013) Biocompatibility of engineered nanoparticles for drug delivery. J Controlled Release 166(2):182–194
5. Canaparo R, Foglietta F, Giuntini F, Della Pepa C, Dosio F, Serpe L (2019) Recent developments in antibacterial therapy: focus on stimuli-responsive drug-delivery systems and therapeutic nanoparticles. Molecules 24(10):1991
6. Hasnain MS, Ahmed SA, Alkahtani S, Milivojevic M, Kandar CC, Dhara AK, Nayak AK (2020) Biopolymers for drug delivery. Advanced biopolymeric systems for drug delivery:1–29
7. Gopi S, Amalraj A, Sukumaran NP, Haponiuk JT, Thomas S Biopolymers and their composites for drug delivery: a brief review. Macromolecular Symposia, 2018, vol 1. Wiley Online Library, p 1800114
8. Fathi R, Mohammadi R (2023) Preparation of pH-responsive magnetic nanocomposite hydrogels based on k-carrageenan/chitosan/silver nanoparticles: antibacterial carrier for potential targeted anticancer drug delivery. Int J Biol Macromol 246:125546
9. Anand R, Kumar A (2021) Significant biopolymers and their applications in buccal mediated drug delivery. J Biomater Sci Polym Ed 32(9):1203–1218
10. Einhorn-Stoll U, Archut A, Eichhorn M, Kastner H (2021) Pectin-plant protein systems and their application. Food Hydrocolloids 118:106783
11. Liu L, Fishman ML, Hicks KB (2007) Pectin in controlled drug delivery–a review. Cellulose 14:15–24
12. Kedir WM, Deresa EM, Diriba TF (2022) Pharmaceutical and drug delivery applications of pectin and its modified nanocomposites. Heliyon 8:9
13. Han SS, Ji SM, Park MJ, Suneetha M, Uthappa UT (2022) Pectin based hydrogels for drug delivery applications: a mini review. Gels 8(12):834
14. Islam MS, Islam MM (2021) Physical and chemical properties of sustainable polymers and their blends. Advances in sustainable polymer composites. Elsevier, pp 37–57
15. Mansor MR, Akop MZ (2020) Polymer nanocomposites smart materials for energy applications. Polymer nanocomposite-based smart materials. Elsevier, pp 157–176
16. Mallakpour S, Hatami M (2019) Fabrication and characterization of pH-sensitive bio-nanocomposite beads havening folic acid intercalated LDH and Chitosan: drug release and mechanism evaluation. Int J Biol Macromol 122:157–167
17. Mohammadzadeh A, Javanbakht S, Mohammadi R (2024) Magnetic alginate core-shell nanoparticles based on Schiff-base imine bonding for pH-responsive doxorubicin delivery system. Colloids Surf A: Physicochemical Eng (**Aspects:134473**)
18. Namazi H (2017) Polymers in our daily life. BioImpacts: BI 7(2):73
19. Seo JS, Whang D, Lee H, Jun SI, Oh J, Jeon YJ, Kim K (2000) A homochiral metal–organic porous material for enantioselective separation and catalysis. Nature 404(6781):982–986
20. Sun Y, Zheng L, Yang Y, Qian X, Fu T, Li X, Yang Z, Yan H, Cui C, Tan W (2020) Metal–organic framework nanocarriers for drug delivery in biomedical applications. Nano-Micro Lett 12:1–29
21. Yang J, Yang YW (2020) Metal–organic frameworks for biomedical applications. Small 16(10):1906846
22. Javanbakht S, Pooresmaeil M, Hashemi H, Namazi H (2018) Carboxymethylcellulose capsulated Cu-based metal-organic framework-drug nanohybrid as a pH-sensitive nanocomposite for ibuprofen oral delivery. Int J Biol Macromol 119:588–596
23. Rodenas T, Luz I, Prieto G, Seoane B, Miro H, Corma A, Kapteijn F, Llabrés i Xamena FX, Gascon J (2015) Metal–organic framework nanosheets in polymer composite materials for gas separation. Nat Mater 14(1):48–55
24. Liu Y, Zhou L, Dong Y, Wang R, Pan Y, Zhuang S, Liu D, Liu J (2021) Recent developments on MOF-based platforms for antibacterial therapy. RSC Med Chem 12(6):915–928
25. Singh N, Qutub S, Khashab NM (2021) Biocompatibility and biodegradability of metal organic frameworks for biomedical applications. J Mater Chem B 9(30):5925–5934
26. Chai Y, Zhang Y, Wang L, Du Y, Wang B, Li N, Chen M, Ou L (2022) In situ one-pot construction of MOF/hydrogel composite beads with enhanced wastewater treatment performance. Sep Purif Technol 295:121225
27. Zhu W, Zhao J, Chen Q, Liu Z (2019) Nanoscale metal-organic frameworks and coordination polymers as theranostic platforms for cancer treatment. Coord Chem Rev 398:113009
28. Shi Y, Liang B, Lin R-B, Zhang C, Chen B (2020) Gas separation via hybrid metal–organic framework/polymer membranes. Trends Chem 2(3):254–269
29. Pettinari C, Tăbăcaru A, Galli S (2016) Coordination polymers and metal–organic frameworks based on poly (pyrazole)-containing ligands. Coord Chem Rev 307:1–31
30. Hamedi H, Javanbakht S, Mohammadi R (2024) In-situ synthesis of copper-gallic acid metal–organic framework into the gentamicin-loaded chitosan hydrogel bead: a synergistic enhancement of antibacterial properties. J Ind Eng Chem 133:454–463

31. Abdelhamid HN (2021) Zeolitic imidazolate frameworks (ZIF-8) for biomedical applications: a review. Curr Med Chem 28(34):7023–7075
32. Darvishi S, Sadjadi S, Heravi MM (2024) Sulfonic acid-functionalized chitosan–metal–organic framework composite for efficient and rapid conversion of fructose to 5-hydroxymethylfurfural. Sci Rep 14(1):5834
33. Darvishi S, Sadjadi S, Monflier E, Heydari A, Heravi MM (2024) Sulfonic acid-functionalized k-carrageenan/Cr-based metal-organic framework: an efficient and recyclable catalyst for fructose conversion to 5-hydroxymethylfurfural. Int J Biol Macromol 264:130555
34. Kim ML, Otal EH, Hinestroza JP (2019) Cellulose meets reticular chemistry: interactions between cellulosic substrates and metal–organic frameworks. Cellulose 26:123–137
35. Nadar SS, Vaidya L, Maurya S, Rathod VK (2019) Polysaccharide based metal organic frameworks (polysaccharide–MOF): a review. Coord Chem Rev 396:1–21
36. Hidalgo T, Giménez-Marqués M, Bellido E, Avila J, Asensio M, Salles F, Lozano M, Guillevic M, Simón-Vázquez R, González-Fernández A (2017) Chitosan-coated mesoporous MIL-100 (fe) nanoparticles as improved bio-compatible oral nanocarriers. Sci Rep 7(1):43099
37. Wang L, Xu H, Gao J, Yao J, Zhang Q (2019) Recent progress in metal-organic frameworks-based hydrogels and aerogels and their applications. Coord Chem Rev 398:213016
38. Hamedi H, Javanbakht S, Mohammadi R (2023) In-situ synthesis of copper-gallic acid metal-organic framework into the gentamicin-loaded chitosan hydrogel bead: a synergistic enhancement of antibacterial properties. Journal of Industrial and Engineering Chemistry
39. Ranjbar E, Namazi H, Pooresmaeil M (2022) Carboxymethyl starch encapsulated 5-FU and DOX co-loaded layered double hydroxide for evaluation of its in vitro performance as a drug delivery agent. Int J Biol Macromol 201:193–202
40. Darvishi S, Javanbakht S, Heydari A, Kazeminava F, Gholizadeh P, Mahdipour M, Shaabani A (2021) Ultrasound-assisted synthesis of MIL-88 (fe) coordinated to carboxymethyl cellulose fibers: a safe carrier for highly sustained release of tetracycline. Int J Biol Macromol 181:937–944
41. Nia SB, Pooresmaeil M, Namazi H (2020) Carboxymethylcellulose/layered double hydroxides bio-nanocomposite hydrogel: A controlled Amoxicillin nanocarrier for colonic bacterial infections treatment. Int J Biol Macromol 155:1401–1409
42. Javanbakht S, Shaabani A (2019) Encapsulation of graphene quantum dot-crosslinked chitosan by carboxymethylcellulose hydrogel beads as a pH-responsive bio-nanocomposite for the oral delivery agent. Int J Biol Macromol 123:389–397
43. Wu C, Liu Q, Chen R, Liu J, Zhang H, Li R, Takahashi K, Liu P, Wang J (2017) Fabrication of ZIF-8@ SiO2 micro/nano hierarchical superhydrophobic surface on AZ31 magnesium alloy with impressive corrosion resistance and abrasion resistance. ACS Appl Mater Interfaces 9(12):11106–11115
44. Joel J, Barminas J, Riki E, Yelwa J, Edeh F (2018) Extraction and characterization of hydrocolloid pectin from goron tula (Azanza Garckeana) fruit. World Sci news 101:157–171
45. Trivedi M, Patil S, Shettigar H, Bairwa K, Jana S, Bairwa K (2015) Spectroscopic characterization of chloramphenicol and tetracycline: an impact of biofield. Pharm Anal Acta 6(395):19–21
46. Borsagli FGM, Ciminelli VS, Ladeira CL, Haas DJ, Lage AP, Mansur HS (2019) Multi-functional eco-friendly 3D scaffolds based on N-acyl thiolated chitosan for potential adsorption of methyl orange and antibacterial activity against Pseudomonas aeruginosa. J Environ Chem Eng 7(5):103286
47. Zhang Y, Jia Y (2018) Synthesis of zeolitic imidazolate framework-8 on polyester fiber for PM 2.5 removal. RSC Adv 8(55):31471–31477
48. Hastuti B, Hadi S (2020) Adsorption of Pb (II) ion using pectin membrane. In: IOP Conference Series: Materials Science and Engineering, vol 1. IOP Publishing, p 012014
49. Dong W, Zhao S, Wang Y, Zhou X, Jiang J, Dang J, Sun D, Dai X, Zhang M, Jiang Z (2023) Stimuli-responsive metal–organic framework hydrogels endow long carbon fiber reinforced polyetheretherketone with enhanced anti-inflammatory and angiogenesis and osteogenesis. Mater Design 225:111485
50. Paul A, Vyas G, Paul P, Srivastava DN (2018) Gold-nanoparticle-encapsulated ZIF-8 for a mediator-free enzymatic glucose sensor by amperometry. ACS Appl Nano Mater 1(7):3600–3607
51. Al-Degs YS, El-Barghouthi MI, El-Sheikh AH, Walker GM (2008) Effect of solution pH, ionic strength, and temperature on adsorption behavior of reactive dyes on activated carbon. Dyes Pigm 77(1):16–23
52. Javanbakht S, Nazari N, Rakhshaei R, Namazi H (2018) Cu-crosslinked carboxymethylcellulose/naproxen/graphene quantum dot nanocomposite hydrogel beads for naproxen oral delivery. Carbohydr Polym 195:453–459
53. Banu AR, Devi MK, Gnanaprabhal G, Pradeep B, Palaniswamy M (2010) Production and characterization of pectinase enzyme from Penicillium Chrysogenum. Indian J Sci Technol:377–381
54. Goldsmith J, Randall N, Ross S (1978) On methods of expressing dissolution rate data. J Pharm Pharmacol 30(1):347–349
55. Ashfaq M, Khan S, Verma N (2014) Synthesis of PVA-CAP-based biomaterial in situ dispersed with Cu nanoparticles and carbon micro-nanofibers for antibiotic drug delivery applications. Biochem Eng J 90:79–89
56. Shen B, Wang Y, Wang X, Amal FE, Zhu L, Jiang L (2022) A cruciform petal-like (ZIF-8) with bactericidal activity against foodborne gram-positive bacteria for antibacterial food packaging. Int J Mol Sci 23(14):7510
57. Xia X, Song X, Li Y, Hou W, Lv H, Li F, Li Y, Liu J, Li X (2022) Antibacterial and anti-inflammatory ZIF-8@ rutin nanocomposite as an efficient agent for accelerating infected wound healing. Front Bioeng Biotechnol 10:1026743
58. Barrenechea V, Vargas-Reyes M, Quiliano M, Milón P (2021) A complementary mechanism of bacterial mRNA translation inhibition by tetracyclines. Front Microbiol 12:682682
59. Brodersen DE, Clemons WM, Carter AP, Morgan-Warren RJ, Wimberly BT, Ramakrishnan V (2000) The structural basis for the action of the antibiotics tetracycline, pactamycin, and hygromycin B on the 30S ribosomal subunit. Cell 103(7):1143–1154
60. Mousavi SA, Janjani H (2018) Antibiotics adsorption from aqueous solutions using carbon nanotubes: a systematic review. Toxin Reviews
61. Ruhal R, Kataria R (2021) Biofilm patterns in gram-positive and gram-negative bacteria. Microbiol Res 251:126829
62. Mai-Prochnow A, Clauson M, Hong J, Murphy AB (2016) Gram positive and Gram negative bacteria differ in their sensitivity to cold plasma. Sci Rep 6(1):38610
63. Sonohara R, Muramatsu N, Ohshima H, Kondo T (1995) Difference in surface properties between Escherichia coli and Staphylococcus aureus as revealed by electrophoretic mobility measurements. Biophys Chem 55(3):273–277
64. Jung WK, Koo HC, Kim KW, Shin S, Kim SH, Park YH (2008) Antibacterial activity and mechanism of action of the silver ion in Staphylococcus aureus and Escherichia coli. Appl Environ Microbiol 74(7):2171–2178
65. Poursadegh H, Amini-Fazl MS, Javanbakht S, Kazeminava F (2024) Magnetic nanocomposite through coating mannose-functionalized metal-organic framework with biopolymeric pectin

hydrogel beads: a potential targeted anticancer oral delivery system. Int J Biol Macromol 254:127702